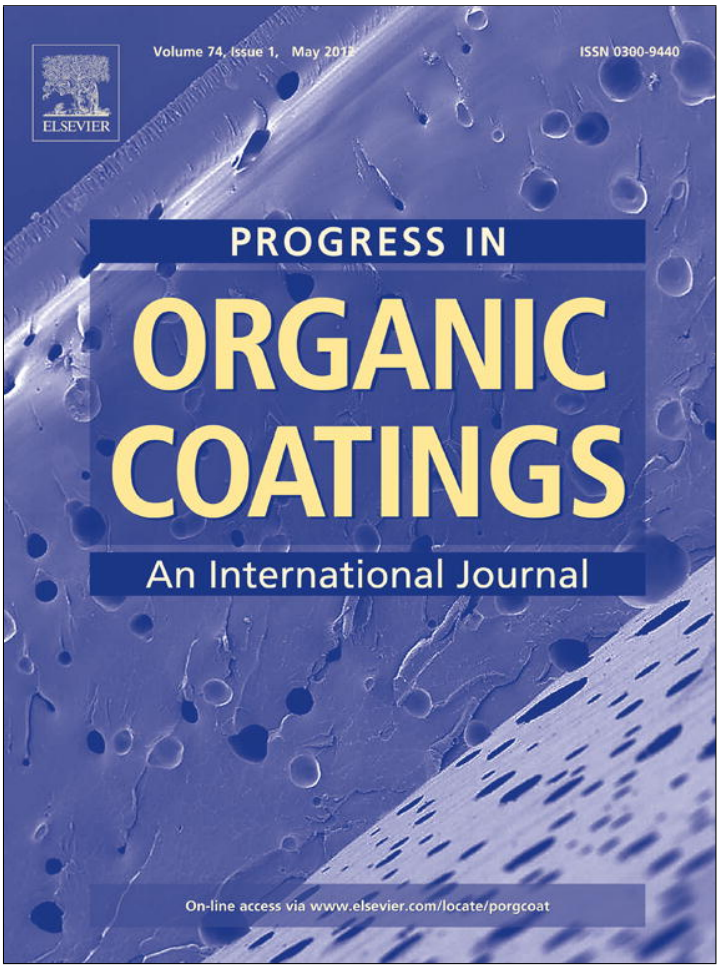

Progress in Organic Coatings 74 (2012) 43–49

Contents lists available at SciVerse ScienceDirect

Progress in Organic Coatings

journal homepage: www.elsevier.com/locate/porgcoat

A comparison of different approaches for depth profiling of films and coatings by confocal Raman microscopy

María de la Paz Miguel, J. Pablo Tomba*

Institute of Materials Science and Technology (INTEMA), National Research Council (CONICET), National University of Mar del Plata (UNMDP), Juan B. Justo 4302, 7600 Mar del Plata, Argentina

ARTICLE INFO

Article history:
Received 25 July 2011
Received in revised form 23 August 2011
Accepted 27 September 2011
Available online 22 October 2011

Keywords:
Confocal Raman microscopy
Depth profiling
Polymer films and coatings
Deconvolution

ABSTRACT

We compare and analyze different approaches to perform depth profiling of polymer films and coatings by confocal Raman microscopy (CRM). Data were generated using three methodologies: conventional metallurgical objectives, oil-immersion optics and numerical post processing of the as-measured intensity profiles, via an optimized deconvolution technique adapted to CRM. A series of bi- and multi-layered polymeric films were used as test systems. Strengths and weaknesses of each methodology are evaluated in terms of delivered depth resolution, signal throughput and flexibility. It is shown that the application of regularized deconvolution on data obtained from dry objectives yielded intensity profiles with a quality comparable, in some cases superior, to those obtained with immersion objectives, with the advantage of being totally non-invasive.

1. Introduction

Confocal Raman microscopy (CRM) is a powerful analytical tool that offers several modes to perform either surface or bulk studies on polymeric films and coatings. Among them, depth profiling allows the nondestructive characterization of transparent samples by exploiting the optical sectioning capabilities of the technique. It is possible to gather spectroscopic information deep within the sample without the need of physical sectioning, which virtually implies no sample preparation. Many polymers used in applications such as protective coatings, adhesives, packaging or drug delivery can be characterized with this methodology, which can be used not only to access to details of structure, but also to monitor time dependent phenomena such as diffusion, segregation, layering, phase transitions or chemical transformations [1–8].

In depth profiling by CRM, the sample is normally examined with a microscope objective, for which diffraction theory predicts a depth (or axial) resolution $\sim\lambda\, n_m/(NA)^2$, where λ is the laser wavelength, n_m is the refractive index of the medium between objective and sample, and NA the objective numerical aperture [9]. Metallurgical (or dry) objectives are widely used in Raman microscopy because of their versatility; as the specimen is probed through air ($n_m \sim 1$), there is no contact with the sample which turns out the exploration totally non-invasive. For visible lasers and metallurgical objectives customary used, nominal values of depth resolution in confocal conditions of about 2 μm are fairly common. However, those values increase *within* the sample, due to spherical aberrations caused by the mismatch in refractive indexes between air and sample (laser refraction). The effect causes not only a significant broadening of the depth response as one probes deeper into the sample but also an artificial compression of the depth scale, making sample features to appear artificially closer to the microscope objective [10]. In addition, deviation of the laser rays from their original path causes a mismatch in the confocal aperture positioning that affects adversely the collection efficiency causing a continuous reduction in the detected intensity with focusing depth [11].

The use of oil-immersion objectives, originally developed for biological applications, overcomes several of those issues. These objectives are designed to operate coupled to the specimen through a liquid layer of the same refractive index; organic oils with refractive index ~1.5 are used with this purpose. This configuration avoids dramatic discontinuities in the refractive index along the laser pathway, helping to reduce spherical aberrations and to keep depth resolution within the sample sharp and nearly invariant. The collection efficiency also improves as immersion objectives have larger NA values than the dry ones.

Unfortunately, immersion optics cannot be applied to the universe of samples, besides the fact they are much more costly than the metallurgical counterparts. One of the main limitations, particularly critical when working with polymers substrates, is the potential risk of sample damage as the coupling fluid is in *direct* contact with the specimen; some strategies to remedy that issue have been suggested, see for instance Refs. [12,13]. Another problem

* Corresponding author.
E-mail address: jptomba@fi.mdp.edu.ar (J. Pablo Tomba).

0300-9440/$ – see front matter © 2011 Elsevier B.V. All rights reserved.
doi:10.1016/j.porgcoat.2011.09.016

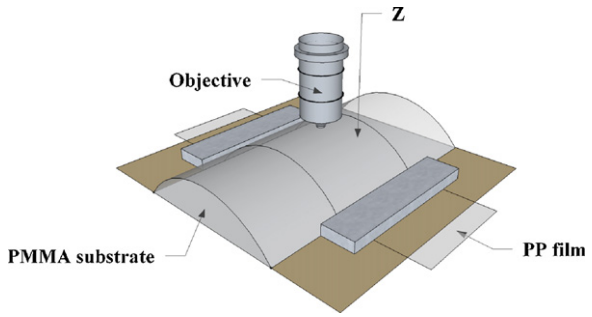

Fig. 1. Sketch of the experimental setup.

is that the oil may also contribute additional overlapping Raman peaks/fluorescence bands. In terms of handling, this class of optics is trickier to use as the objective has to be brought very close to the specimen to focus (short working distance) and the focal plane is so shallow that focusing itself can be difficult.

A different non-instrumental strategy, recently considered in CRM, is the use of numerical corrections to improve data precision and quality [14,15]. We could, for instance, acquire data with a metallurgical objective and remove optical distortions by numerical post-processing. This concept has been employed by Reinecke and coworkers to correct intensity profiles of a modifier in a polymer film, assuming a pre-established shape for the modifier distribution [14]. More recently, our group proposed a general formulation based on regularized deconvolution to correct intensity profiles, with the advantage of imposing no restrictions of shape to the recovered solution [16]. Overall, the core of these methods relies on a precise knowledge on how the depth response is distorted by optical/instrumental conditions, which is usually described by the instrumental Point Spread Function (PSF). What is challenging in CRM with dry objectives is that PSF is not invariant but it changes with focusing depth, which is rather different from other closely related techniques, like confocal fluorescence microscopy (CFM), which employ numerical post-processing to improve image quality but under the strict assumption of invariant PSF [17].

The objective of this work is to compare the quality of results, in terms of depth resolution and signal intensity, produced by the three approaches for depth profiling by CRM above described: dry and oil-immersion techniques and data post-processing by regularized deconvolution [15]. The test sample under study was a bilayered laminate built by supporting a thin polypropylene (PP) film onto a much thicker poly (methyl metacrylate) (PMMA) substrate. PP films with different thickness and several acquisition conditions (type of objective, size of confocal aperture) were tested. We also analyze results obtained from a polymer multilaminate, consisting on a layer of polyethylene (PE) sandwiched between two PP films, which is not only a more challenging sample to compare methodologies but also a situation frequently found in practice.

2. Experimental

The bi-layer system studied was built by supporting a thin polypropylene (PP) film of known thickness onto a much thicker poly (methyl methacrylate) (PMMA) substrate. Three commercial PP films, with thicknesses of 25, 50 and 80 μm, as measured with a Mitutoyo micrometer (model 395-271) with ±1 μm precision, were used. The PMMA substrate was built with a smooth convex curvature on top, which combined with the tensile force applied by clamps to the film edges assured a good film/substrate contact, see Fig. 1. The multilayered material was made of a 25 μm layer of PE (polyethylene) sandwiched between two PP layers 25 μm thick. The whole system was supported onto the same PMMA substrate as explained earlier.

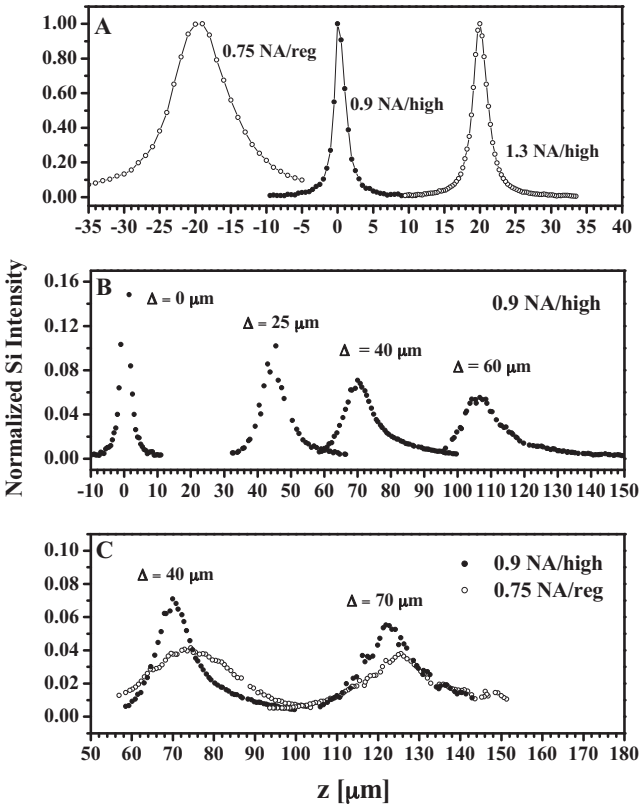

Fig. 2. (A) Point Spread Function in the absence of refraction, normalized to maximum intensity, for three objective/confocality combinations, 0.9 NA/high (center), 0.75 NA/regular (left, shifted by −20 units) and 1.3 NA/high (right, shifted by 20 units). (B) Actual PSFs within the material, normalized to unit area, for one of the dry objectives and different values of focusing depth (Δ). The curve at $\Delta = 0$ correspond to the PSF with no refraction shown in (A). (C) PSF values obtained for two focusing points with different dry objectives/confocality combinations.

Raman spectra were collected with a Renishaw inVia Reflex spectrometer system equipped with a 514 nm wavelength Ar laser as excitation source (50 mW) in combination with a grating of 2400 grooves/mm. Confocality for light collection was achieved by tuning the pixel binning of the spatial dimension of the CCD and the aperture of the spectrograph entrance slit. The Wire 3.2 software allows a common user to toggle between two preset confocality configurations, *high* (3 pixels of the CCD, 20 μm slit opening) and *regular* (9 pixels of the CCD, 65 μm slit opening). These configurations are analogous to *small* and *large* confocal apertures in pinhole based instruments. Three Leica microscope objectives were used in this work. Two were metallurgical (N PLAN), 0.9 NA (100×) and 0.75 NA (50×) and one for oil-immersion (HCX PL FLUOTAR), 1.3 NA (100×), to be used in conjunction with a coupling fluid with $n = 1.52$. Depth-profiling was carried out by mounting the samples on a microscope stage which is displaced vertically in steps of 0.5 or 1 μm controlled by software with 0.1 μm precision. Intensity depth-profiles were measured by taking Raman spectra at different depths, employing two 5-s acquisitions for each data point and 10% laser power.

3. Results and discussion

3.1. Depth resolution of each methodology

We start characterizing the operative values of depth resolution for the different approaches employed. Depth resolution is usually characterized from the full width at the half maximum (FWHM) of the instrumental PSF. A classic test to determine PSF

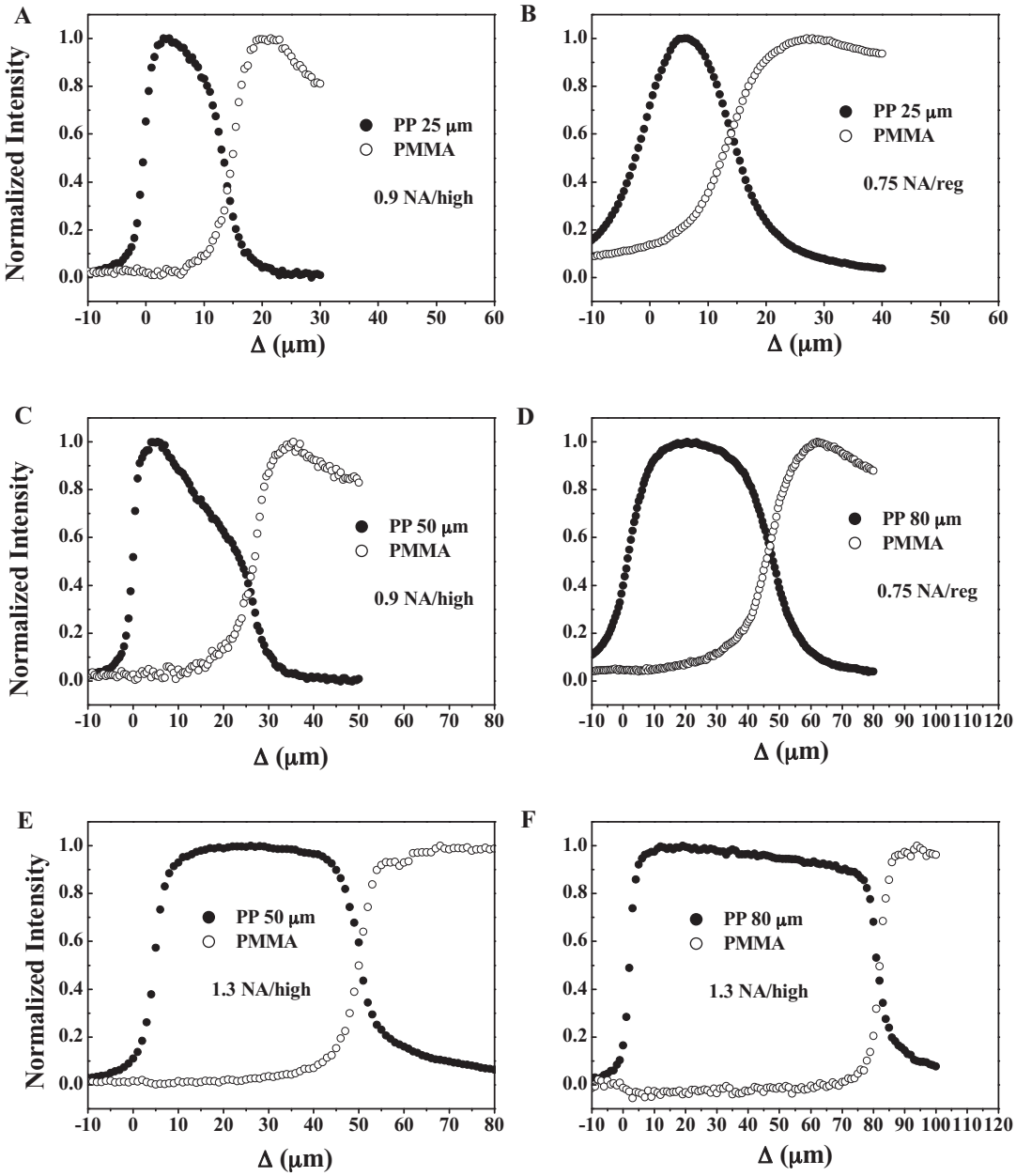

Fig. 3. Profiles of PP films supported onto a PMMA substrate, as taken with the instrumental configurations indicated in the plot. PP film thicknesses are also indicated. (A–D) Data acquired with dry optics and (E and F) data obtained via immersion optics.

in Raman microscopy involves the *z*-scanning of a mirror-polished silicon wafer, normally to its surface, and the representation of the intensity of the 520 cm^{-1} Raman peak as a function of the distance. As silicon is strongly absorbent, it behaves essentially as a material of infinitesimal thickness providing a punctual response. Fig. 2(A) shows the curve obtained for three objective/confocality combinations, normalized to maximum intensity and shifted along the horizontal scale by 20 units to left (0.75 NA) and to right (1.3 NA). Although other combinations are possible, those chosen represent the boundaries between optimum depth resolution (1.3/high or 0.9 NA/high) and optimum signal (0.75 NA/regular, see below). We see that all the responses are nearly symmetrical. The oil-immersion and 0.9 NA dry objective, combined with a small confocal aperture, yielded nearly the same response, characterized by a FWMH of about 2.5 μm. The combination 0.75 NA/regular yielded a broader response (9.3 μm FWHM), due to the lower NA and larger confocal aperture used. All these PSFs represent the instrumental response in the absence of refraction and reflect a combination of diffraction limited illumination (objective and laser wavelength dependent), size of confocal aperture in the collection path and non-idealities of the optical system.

Fig. 2(B) shows actual PSFs well within the material for one of the dry objectives (0.9 NA). The determination of these PSFs is not trivial and involves a carefully designed experiment consisting in the depth slicing of a silicon wafer buried in a thin molded polystyrene wedged-shape film; more details will be given in a forthcoming publication [18]. In this representation, Δ refers to the nominal focusing depth, as obtained from the scale of the microscope platform, while *z* refers to the true axial scale [10]. $\Delta = 0$ μm corresponds to focusing on the sample surface and $\Delta > 0$ to focus points deep within the material. The data shown correspond to three values of Δ, normalized to unit area where the PSF at $\Delta = 0$ μm represent the response with no refraction shown before. In the presence of spherical aberrations (refraction) the PSF

changes appreciably in shape with depth, turning asymmetric. We see that the depth responses lie much deeper than the point where the laser beam was originally focused, i.e., Δ and z scales are different, and they span over much wider regions (tens of microns) than the original diffraction-limited response at $\Delta = 0$ μm. These effects, have their root in the mismatch of refractive index between air and polymer sample, as predicted by geometric optics theory [10]. For the immersion optics, as refraction is minimized, the PSF shown in Fig. 2(A) as 1.3 NA/high should represent quite well the response within the material, at any depth.

Fig. 2(C) shows PSF values measured with dry objectives under different instrumental conditions, for two focusing points. At $\Delta = 40$ μm, the response of the 0.9 NA/high configuration is sharper than that obtained with the 0.75 NA/regular one, as a result of the differences shown by the original free-of-refraction responses in Fig. 2(A). However, when focusing deeper within the sample, i.e., $\Delta = 70$ μm, the broadening by refraction dominates and the responses become comparable. These results show that working with dry objectives in optimum confocal condition (0.9 NA/high) provides the highest possible depth discrimination, if we work not very far from the sample surface. On the other hand, the small confocal aperture required by the optimum confocal condition reduces the amount of signal collected by the detector, extending acquisition times. In fact, there is a compromise between depth resolution and time of analysis that will be more deeply analyzed in the next section.

3.2. Depth profiling of bilayered systems

Fig. 3 shows intensity profiles for both components of the bilayered system, PP and PMMA, as obtained in confocal depth profiling experiments, all of them normalized to unity. These profiles were constructed by using component analysis (or linear decomposition), a methodology that assembles each local spectrum from a linear combination of spectra of individual components [19]. As the method employs the whole Raman profile, it yields data much less noisy, more suitable for our analysis, than those obtained by plotting the intensity of a single Raman peak. The weight coefficients of the linear expansion directly measure the relative contribution of individual components to the global spectrum. This information is plotted versus the focusing depth to generate the corresponding in-depth confocal profile, where the zero in the Δ scale corresponds to the PP film outer surface.

The top figures correspond to profiles of a PP film 25 μm thick, supported onto a PMMA substrate, as taken with different metallurgical objectives/confocality combinations, 0.9 NA/high and 0.75 NA/regular. We observe that in both experiments the apparent thickness of the PP film is less than the real value and that the PP/PMMA interface, expected to be sharp, appears instead artificially broadened. Both effects can be understood in terms of the behavior shown by the PSFs in Fig. 2(B). The broadening observed in the air/PP interface is essentially determined by the combination laser/objective/confocality used, as seen Fig. 2(A), with no influence of refraction as this effect operates well below the sample surface. The difference in the extent of broadening of that interface observed between Fig. 3(A) and (B) is due to larger laser spot size and confocal aperture used in the 0.75 NA/regular combination, which increases the collection volume, as was seen in Fig. 2(C). However, the behavior of PSF shown by that figure predicts that the potential enhancement in depth discrimination that one could obtain using the 0.9 NA/high combination is lost when we probe deeper within the sample due to the dominance of the refraction interference.

All these features are also observed in Fig. 3(C) and (D), for PP films 50 μm and 80 μm thick. Additionally, Fig. 3(C) exemplifies the dramatic fall in collected intensity with focusing depth

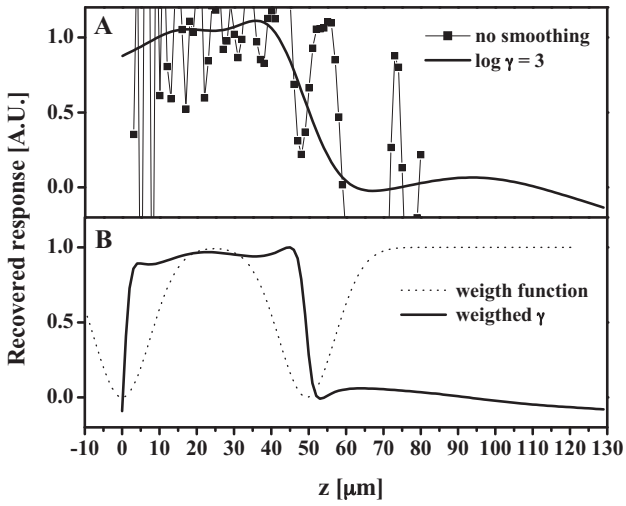

Fig. 4. (A) Recovered signal with and without regularization (solid line and symbols, respectively), as obtained by deconvolution of the dry response of a 50 μm thick PP film. (B) Recovered signal obtained by applying a weighting factor to the γ parameter along the depth scale (solid line); the dotted line shows the profile of the weighting function.

typically observed in depth profiling with dry objectives. The effect is also attributed to laser refraction and the distortion suffered by the scattering volume collected by the confocal aperture, which improperly blocks part of the Raman scattering that reaches the detector [11]. We also see that the effect is less evident in Fig. 3(D), due to the larger confocal aperture employed in the regular configuration.

Another important aspect in these experiments is the overall signal intensity, directly related with the collection time. Overall, the 0.75 NA/regular combination yields about 10 times more photons than the 0.9 NA/high combination, i.e., with the 0.75 NA/regular combination the time of the experiment can be reduced by a factor of 10 over the 0.9 NA/high. In summary, although the 0.9 NA/high combination yields a nominally higher depth resolution compared with the 0.75/regular setup, it happens at the expense of working with overall lower Raman intensities and more pronounced falls as we focus deeper into the sample.

Fig. 3(E) and (F) corresponds to intensity profiles taken with an immersion objective, in optimum confocal conditions (1.3 NA/high). We have omitted in those figures the oil profile, to focus our attention on the PP and substrate responses. We see that in this case, the profiles obtained for both components are much more realistic than those obtained under refraction interference: the outer and inner surfaces of the PP film look sharp and the real thickness of the PP film can be directly inferred from the as-measured profile. Unlike what occurs with dry objectives, there is almost no fall in collected intensity with focusing depth; the small drop observed is more likely due to lack of film transparency and/or internal losses. The signal intensity was in between those we collected with dry optics: the 1.3 NA/high configuration yields about 4 times more intensity that 0.9 NA/high, but about 2.5 times lower those typically obtained with the 0.75 NA/regular setup. Clearly, measurements made with immersion objectives captures very well all the details of the real system and represent the best choice except in situations where oil is detrimental to the sample or when we need to probe depths >150 μm, beyond the typical working distance of the high NA immersion objectives.

3.3. Deconvolution of as-obtained dry depth profiles

A formulation for deconvolution in the context of the present problem has been given in a recent publication [15]. Briefly, we

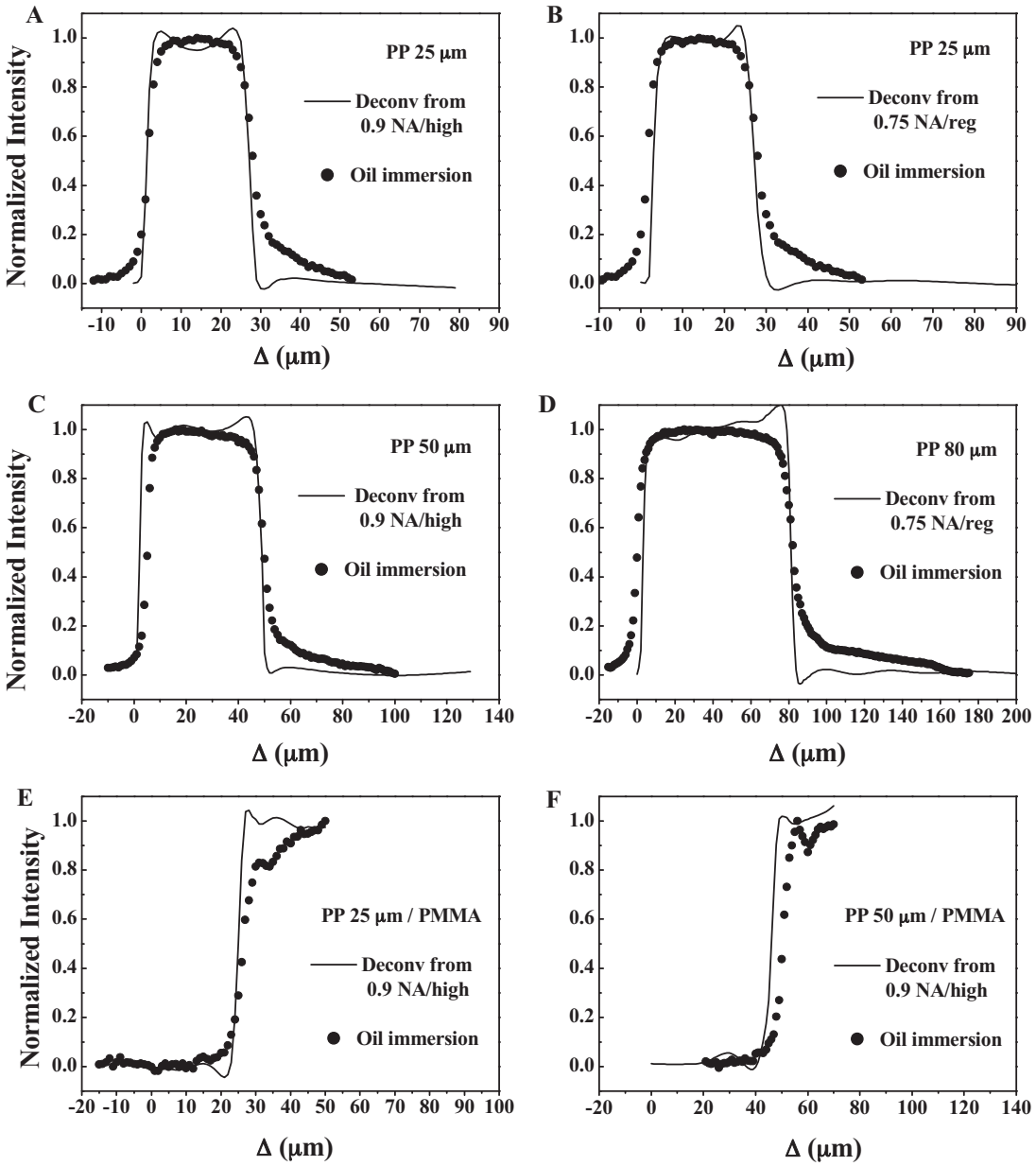

Fig. 5. A comparison between numerically corrected profiles with those obtained with oil-immersion objectives. Film thicknesses and instrumental conditions are indicated in the plot. Deconvolution was only applied to the dry responses. (A–D) PP responses and (E and F) PMMA responses.

assume that the experiment can be described with a convolution integral $I_m(\Delta) = \int_0^\infty B(\Delta, z) I_r(z) dz$, that relates as measured (I_m) and real (I_r) responses, through the kernel B, which represents the PSF. Notice that the domains of those functions, Δ and z, respectively, are different due to the distortions on the depth scale originated by refraction. By inverting the problem, we can deconvolve the real response I_r from the distorted as-measured signal I_m. A key element in this calculation is the use of models for an accurate prediction of PSF, an issue extensively discussed in earlier publications [20]. The model used here relies upon describing the effect laser refraction and the confocal aperture on the original diffraction limited response, which is empirically determined, as shown in Fig. 2(A) [15]. Once characterized for a given set of instrumental conditions, that function is distorted by refraction following the treatments of Everall and Batchelder [10,11], described in earlier papers. The kind of output produced by the model is similar to that shown in Fig. 2(B) and (C), see Ref. [16]. In summary, for a given set of operative conditions (objective, sample refractive index, and confocality) and focusing depth (Δ), the PSF function can be defined and readily calculated in the z domain.

Another key element in the deconvolution process is a regularization scheme for the obtained solution. Overall, the problem posed by direct solving the discrete form of the convolution integral is ill-conditioned and typically yields a response with abrupt oscillations. Fig. 4 exemplifies signals obtained by deconvolution of depth profiles of a thin film, 50 μm thick, where the response to be recovered is expected to present the same features that the data shown in Fig. 3 for oil-immersion objectives, i.e., two sharp transitions at about 0 and 50 μm, connected by a flat region. Without regularization, the direct solution of the problem is noisy and useless, as seen in Fig. 4(A) with symbols. A more realistic response was obtained by including a regularization parameter (γ) to smooth the solution, see Fig. 4(A), solid line; details about how γ was included

in the calculations are given elsewhere [15]. However, smoothing may artificially mask abrupt changes in Raman intensity associated to genuine sample features, such as edges, interfaces or phase transitions. To avoid that problem, we proposed a scheme that ponders the relative amount of smoothing along the z coordinate, in order to make regularization strong where the signal is presumed to be smooth and weak where the signal changes rapidly, i.e., edges, interfaces, transitions. The dotted line in Fig. 4(B) represents the weight function applied to γ, $1 - \sum_j e^{-(z-z_{\gamma,j})^2/2\sigma^2_{\gamma,j}}$, designed to make smoothing null at the function minima and to allow maximum regularization when the function value is close to unity; details about how that function was implemented in the calculations are given elsewhere [15]. Thus, while z_γ fixes the point of minimum regularization (or maximum change in intensity), σ_γ measures how fast regularization increases at both sides of that point. Defined in this way, the weight function is characterized by a set of z_γ/σ_γ parameters whose values are determined from the original experimental data (see below). Finally, an estimation for an optimum amount of global regularization (γ) was obtained by applying the General Cross Validation technique (GCV, see details in Ref. [21]). The solid line in Fig. 4(B) shows an intensity profile corrected with this methodology where we can see that all the expected film features are very well recovered.

We applied this procedure to the data shown in Fig. 3 in order to obtain a more realistic intensity response. In these systems, as the original data reflect the presence of two interfaces, air/sample and PP/PMMA, two points of maximum change (or minimum regularization) were selected. The first one was placed at $z_\gamma = 0$; the second one was obtained from the first derivative of the raw profile and translated to the z domain by a factor of 1.7–1.8; that factor accounts for the apparent compression due to refraction shown by Δ in a medium with $n \sim 1.5$ [15]. Values of σ_γ in the range 10–20 μm usually yield good results for these systems [15]. The application of the GCV method yielded $\log(\gamma)$ values in the range 1.5 and 2.5. Overall, these values are a rather good estimation for γ and yield a nice quality of data reconstruction, however somewhat better results were obtained with a bit larger $\log(\gamma)$ values (2.5–3 range), which is not surprising as GVC tends to underestimate the optimum amount of regularization. Other parameters used in the calculations were $n = 1.50$ for the polymer media, NA = 0.9 and 0.75 for dry objectives, and radius of confocal apertures (Φ) of 1.0 and 6.0 μm for 0.9 NA/high and 0.75 NA/regular combinations [16].

Fig. 5 shows a direct comparison between recovered profiles in several acquisition conditions, and those obtained with the best possible depth resolution achievable in diffraction-limited Raman microscopy, i.e., 1.3 NA/high configuration. Fig. 5(A–D) shows the response of the PP films while Fig. 5(E) and (F) shows that of the PMMA substrate. We can see that in all the cases the numerically corrected results are in excellent agreement with those measured with the oil-immersion objective, despite of the ripples observed, typical of problem inversion. Indeed, most of them are even more realistic than those obtained with immersion optics; for instance, the interfaces look sharper in the corrected results than in the data obtained with the oil. The latter is explained by the fact that the model used to describe PSF in the deconvolution process accounts for most of the sources of broadening, i.e., diffraction, optics non-idealities, and refraction, while the inherent broadening shown in Fig. 2(A) remains in the oil-immersion experiment. A deconvolution step with an invariant PSF could correct for this broadening but without avoiding the complication of working with the coupling oil. As can be seen by comparing Fig. 5(A) and (B), the quality of the reconstruction does not depend much on acquisition conditions, which means that we can safely work with a 0.75 NA/regular configuration without sacrificing data precision and with 2.5-fold increase in signal intensity with respect to the oil-immersion optics.

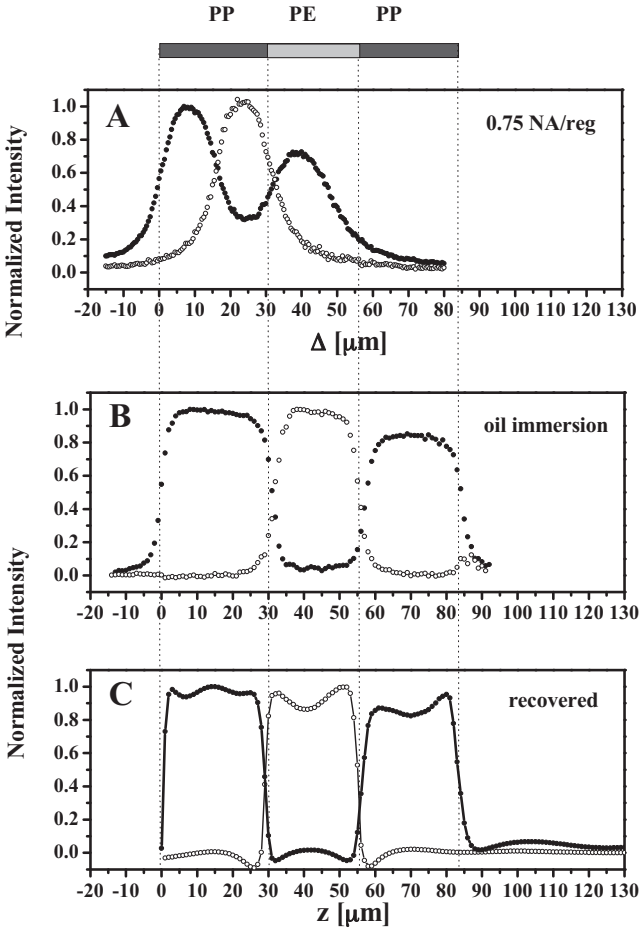

Fig. 6. Depth profiles of a polymer multilaminate obtained with the three methodologies. (A) Dry optics; (B) oil-immersion optics and (C) deconvolution of data shown in (A).

3.4. Depth profiling of polymer multilaminates

A more challenging test for deconvolution is its application to the study of a multilayered laminate, built in this case by a PE layer 25 μm thick sandwiched between two other PP films of about the same thickness. Fig. 6(A) shows the as measured response corresponding to all the film components, as obtained with the 0.75 NA/regular combination, the combination that offers better signal-to-noise ratio. The data show the features and distortions already discussed in Fig. 3, i.e., artificially rounded transitions and distortions in the apparent film layers. A much more realistic response is obtained with the oil-immersion objective, with all the film layers well resolved and with realistic dimensions, as shown by Fig. 6(B). The application of deconvolution to the data shown in Fig. 6(A) yielded the results shown in Fig. 6(C). Deconvolution and model parameters (σ_γ, z_γ, γ, NA, Φ) were chosen as before; the refractive index of the medium was assumed to be uniform (1.5). It can be seen that the numerical treatment corrects the original highly distorted data producing a very realistic response, comparable to that obtained with immersion optics. Remarkably, it was done from original data obtained in technically poor confocal conditions, with a low NA objective, but with excellent signal-to-noise ratio throughout the whole experiment.

4. Conclusions

We have compared three approaches for CRM depth profiling by optical sectioning. The results obtained with standard dry

optics showed substantial degradation in depth resolution, intensity losses, as well as foreshortening of the depth scale, well know effects attributed to the mismatch of refractive indexes between propagating medium and sample. Degradation is substantial even working in confocal conditions. The use of immersion optics provided much better results in terms of both depth resolution and the absence of optical artifacts; however, the presence of organic fluids in direct contact with the sample and the necessity of specialized and delicate objectives hinder a widespread utilization of the methodology. The application of regularized deconvolution on data obtained from dry objectives yielded intensity profiles with a quality comparable, in some cases superior, to those obtained with immersion objectives. The possibility of working with higher signal intensity combined with a variety of objectives, including those of long working distance class, imposes no limits to the universe of systems to be examined.

On the base of this comparison, deconvolution emerges as a truly non-invasive generalized alternative for in-depth sample exploration. The numerical correction has, however, some limitations. One of them, as occurs in CFM, is the assumption of uniform refractive index for the sample, which might limit the analysis of complex heterogeneous substrates with large variations in that property. There exists, however, a vast range of transparent materials susceptible to be depth-profiled with n values narrowly distributed around 1.5. In other cases, as the use of the methodology to trace the distribution of species (i.e., additives, modifiers) in a host matrix, it can be safely carried out assuming that the presence of those species does not change appreciably the average refractive index.

An ultimate goal is to use deconvolution routinely, as part of the CRM instrumentation, like occurs in wide-field or confocal fluorescence microscopy. To reach that point, a reliable prediction of PSF in a variety of instrumental conditions is central. Although substantial progress has been made in CRM in terms of PSF modeling [20,22], some further improvements are still needed, see for instance Ref. [20]. In this sense, direct access to PSF through experimental data of the type shown in Fig. 2(A) and (B), presented here for the first time, constitute an invaluable tool to improve existing PSF models [23]. The analysis of other deconvolution techniques besides regularization, many of them included in commercial packages [17], is a second issue yet to be explored.

References

[1] O.S. Fleming, F. Stepanek, S.G. Kazarian, Macromol. Chem. Phys. 206 (2005) 1077.
[2] J. Sacristan, H. Reinecke, C. Mijangos, S. Spells, J. Yarwood, Macromol. Chem. Phys. 210 (2009) 549.
[3] J.P. Tomba, L. Arzondo, J.M. Carella, J.M. Pastor, Macromol. Chem. Phys. 208 (2007) 1110.
[4] B. Marton, L.G.J. van der Ven, C. Otto, N. Uzunbajakava, M.A. Hempenius, G.J. Vansco, Polymer 46 (2005) 11330.
[5] F. Belaroui, Y. Grohens, H. Boyer, Y. Holl, Polymer 41 (2000) 7645.
[6] W.R. Zhanga, C. Loweb, R. Smitha, Prog. Org. Coat. 66 (2009) 141.
[7] A. Joachimiak, T. Halamus, P. Wojciechowski, J. Ulanski, Macromol. Chem. Phys. 206 (2005) 59.
[8] G. Lorenzetti, J. Striova, A. Zoppi, E.M. Castellucci, J. Mol. Struct. 993 (2011) 97.
[9] C.B. Juang, L. Finzi, C.J. Bustamante, Rev. Sci. Instrum. 59 (1988) 2399.
[10] N. Everall, Appl. Spectrosc. 54 (2000) 773.
[11] K.J. Baldwin, D.N. Batchelder, Appl. Spectrosc. 55 (2001) 517.
[12] J. Vyorykka, J. Halttunen, H. Iitti, J. Tenhunen, T. Vuorinen, P. Stenius, Appl. Spectrosc. 56 (2002) 776.
[13] J.P. Tomba, J.M. Pastor, Macromol. Chem. Phys. 62 (2008) 817.
[14] A. Gallardo, S. Spells, R. Navarro, H. Reinecke, J. Raman Spectrosc. 38 (2007) 880.
[15] J.P. Tomba, M.P. Miguel, C.J. Perez, J. Raman Spectrosc. 42 (2011) 1330.
[16] J.P. Tomba, G. Elicabe, M.P. Miguel, C.J. Perez, Appl. Spectrosc. 65 (2011) 342.
[17] J.B. Sibarita, Adv. Biochem. Eng./Biotechnol. 95 (2005) 201.
[18] M.P. Miguel, J.P. Tomba, J. Raman Spectrosc., in preparation.
[19] J.P. Tomba, J. Polym. Sci.; Part B: Polym. Phys. 43 (2005) 1144.
[20] L.M. Arzondo, J.P. Tomba, J.M. Pastor, Appl. Spectrosc. 61 (2007) 177.
[21] G.H. Golub, M. Heath, G. Wahba, Technometrics 21 (1979) 215.
[22] C. Sourisseau, P. Maraval, Appl. Spectrosc. 57 (2003) 1324.
[23] M.J. Nasse, J.C. Woehl, S. Huant, Appl. Phys. Lett. 90 (2007) 031106.